Available online at www.sciencedirect.com
SCIENCE DIRECT®
PERGAMON
International Journal of Heat and Mass Transfer 46 (2003) 3069–3081
International Journal of HEAT and MASS TRANSFER
www.elsevier.com/locate/ijhmt

The influence of heat on the 3D-transition of the von Kármán vortex street

W.J.P.M. Maas, C.C.M. Rindt *, A.A. van Steenhoven

Energy Technology Division, Department of Mechanical Engineering, Eindhoven University of Technology, WH-3.127, P.O. Box 513, NL-5600 MB Eindhoven, Netherlands

Received 16 November 2001; received in revised form 26 November 2002

Abstract

The wake behind a horizontally mounted heated cylinder with circular cross-section is visualised using an electrochemical tin precipitation method. In the experiments Re_D and Ri_D, both based on main stream properties, were set to 117 and varied between 0 and 1.5, respectively. The wake becomes 3D from $Ri_D \approx 0.3$. For small Richardson values ($Ri_D < 1$), the warm fluid is initially collected in the coherent vortex structures shed from the cylinder. Further downstream thermal plumes originate from these structures. For larger Richardson values ($Ri_D > 1$), the upward buoyancy force seems to prevent the formation of the coherent vortex structures and the plumes are already formed close behind the cylinder. The spanwise positions at which the plumes originate, are determined by the occurrence of 3D flow structures at the rear end of the cylinder. The distance between these structures is typically $1.8D$ and independent of the Richardson number.

Keywords: Cylinder; Mixed convection; Three-dimensional; Transitional

1. Introduction

For moderate flow velocities around a horizontally mounted heated cylinder with circular cross-section, the strength of the buoyancy induced convection flow can be of the same order of magnitude as the forced convection flow. The interaction between these two types of convection changes the mixing properties of the flow compared to the purely forced convection case. This mixing process is of interest in several applications like, for example, in electronics cooling, where the flow behind a cooled component strongly influences the cooling behaviour of more downstream placed components. In the current investigation the influence of heat on the coherent vortex structures in the laminar shedding regime behind a horizontally mounted heated cylinder with circular cross-section, that is exposed to a horizontal uniform cross-flow, is investigated (Fig. 1).

When the so-called Boussinesq approximation [4] is applied to the current flow problem, the following dimensionless conservation equations for mass, momentum and energy can be formulated:

$$\nabla \cdot \mathbf{u} = 0, \tag{1}$$

$$\frac{\partial \mathbf{u}}{\partial t} + \mathbf{u} \cdot \nabla \mathbf{u} = -\nabla p + \frac{1}{Re_D} (\nabla)^2 \mathbf{u} - Ri_D \Theta \mathbf{g}, \tag{2}$$

$$\frac{\partial \Theta}{\partial t} + \mathbf{u} \cdot \nabla \Theta = \frac{1}{Re_D Pr} (\nabla)^2 \Theta, \tag{3}$$

with $Re_D = U_0 D/\nu$ the Reynolds number, $Ri_D = Gr_D/Re_D^2 = g\beta \Delta T D/U_0^2$ the Richardson number, $Gr_D = g\beta \Delta T D^3/\nu^2$ the Grashof number, $Pr = \nu/\kappa$ the Prandtl number, β the expansion coefficient, κ the thermal diffusivity, g the gravity constant, $\mathbf{g} = (0, -1)^T$ the dimensionless gravity vector, $\Theta = (T - T_1)/(T_0 - T_1)$ the dimensionless temperature, $\mathbf{u}$ the dimensionless velocity and p the dimensionless pressure.

* Corresponding author. Tel.: +31-40-247-2978; fax: +31-40-243-3445.
E-mail address: c.c.m.rindt@tue.nl (C.C.M. Rindt).

0017-9310/03/$ - see front matter © 2003 Elsevier Science Ltd. All rights reserved.
doi:10.1016/S0017-9310(03)00076-0

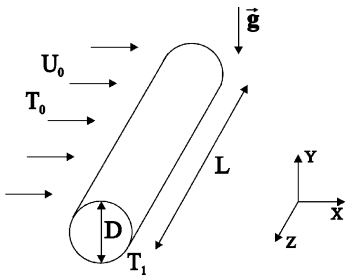

Fig. 1. Problem definition.

From these equations it can be seen that the character of the flow depends on the dimensionless parameters Re_D, Ri_D and Pr. For the currently applied temperature differences between the cylinder and the free-stream the viscosity for water varies appreciably and the usage of an effective Reynolds number, as employed in [12,13], is possibly more appropriate. The employment of an effective Reynolds number will be dealt with more extensively in Appendix A. In the remainder of the main text all mentioned values for the Reynolds, Richardson and Prandtl numbers are based on the free-stream fluid properties.

By taking the curl ($\nabla\times$) of the momentum equation and using the incompressibility constraint, an equation for the vorticity can be derived,

$$\frac{D\boldsymbol{\omega}}{Dt} = \frac{\partial\boldsymbol{\omega}}{\partial t} + \mathbf{u}\cdot\nabla\boldsymbol{\omega} = (\boldsymbol{\omega}\cdot\nabla)\mathbf{u} - Ri_D\nabla\Theta\times\mathbf{g} + \frac{1}{Re_D}\nabla^2\boldsymbol{\omega}. \quad (4)$$

Kieft [1] showed that for $Re_D = 75$, $0 < Ri_D < 1$ and $x/D < 25$ the wake was periodic and 2D. Despite the upward buoyancy force, the vortex street showed a negative deflection. Furthermore the lower vortices appeared to rotate in clockwise direction around the upstream upper vortices (see for both of these phenomena also Fig. 5). From vorticity measurements and numerical simulations it followed that the baroclinic vorticity production resulted in an increase of the upper vortex strength and a decrease of the lower vortex strength. With point-vortex simulations it was shown that both of the above described phenomena could be explained by this strength difference.

In the unheated cylinder case ($Ri_D = 0$) the nominally 2D flow becomes 3D for $Re_D \approx 140$–194, when so-called vortex loops result in streamwise vorticity-components in the von Kármán-vortex street (mode A-instability, see [5]). However, for the heated cylinder case an early transition takes place towards 3D. For $Re_D = 75$ and $Ri_D > 1$ thermal plumes escape from the vortices at some distance downstream of the cylinder. This location is shifted into the direction of the cylinder for an increasing addition of heat (larger Richardson values), see [3]. Because of these secondary structures the wake is no longer 2D here.

In the current investigation the influence of cylinder heating on the 3D-transition of the vortex street will be investigated further. In the experiments Ri_D is varied between 0 and 1.5 while Re_D is fixed at 117. The Prandtl number is constant because all the experiments are carried out in water. To extend the results to other Re_D, also a few experiments are done at $Re_D = 102$ and 75 for different Ri_D.

2. Experimental device and techniques

2.1. Experimental set-up

The experiments are carried out in a towing tank with dimensions length × width × height = 500 × 50 × 75 cm^3. In this configuration the water is at rest and the cylinder is translated with a constant velocity. The cylinder has length $l = 495$ mm and diameter $D = 8.5$ mm ($l/D = 58$), see Fig. 2 (see also [2]).

The test section consists of 15 mm thick glass windows, held together by a steel frame, so the towing tank is optically accessible from all directions. The cylinder is

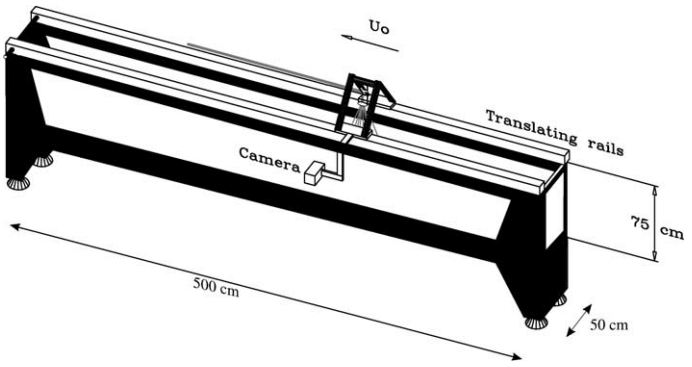

Fig. 2. Towing tank construction with the translating system.

positioned between two Perspex plates, which are connected to a stiff construction on which different kinds of measuring equipment, like cameras and light sources can be placed. The stiff construction can be translated along two rails that are mounted on top of the water tank. The Perspex plates are constructed in such a way that minimum disturbances are created and oblique vortex shedding is suppressed [7]. Furthermore, they insulate the cylinder ends and act as a barrier for influences of temperature gradients in the vicinity of the side-walls of the towing tank.

A cylindrical heating element with diameter 6.35 mm is used to obtain the desired cylinder wall temperature. Around the heating element two copper shields are mounted of which the inner shield has an outer diameter of 8 mm and the outer shield of 8.5 mm. The outer shield has a surface roughness of 0.5 μm. The copper shields damp fast temperature fluctuations and smear out spanwise temperature gradients. To measure the temperature, three thermocouples are positioned between the two shields.

The distance between the cylinder and the bottom of the water tank and the free surface is, respectively, 25D and 50D. According to [8] blockage effects become negligible for distances larger than 20D. The effect of a free-surface, especially for heat induced flows, is less investigated. However, it is assumed that a distance of 50D is enough to rule out any influence on the buoyancy induced transition processes as investigated in the present study. The main source of error in the free-stream velocity is a result of the background velocity in the water tank, which is caused by temperature differences in the water, e.g. the laboratory room. By conditioning this room and by thermally insulating the tank from the room, the background velocity could be minimised to 0.2 mm/s. Together with the other error sources, this means an error in the measured velocity (at $Re_D = 117$) of $\pm 2.0\%$. The wavelength of this background velocity was about the tank width, 50 cm.

As a result of the circumferentially varying heat transfer coefficient the temperature difference between the front and the rear end of the cylinder is 2% of the temperature difference $T_1 - T_0$. The spanwise temperature variation is assumed to be an order of magnitude smaller than the circumferential variation. The noise in the temperature signal is limited to ± 0.05 K.

The frequency and amplitude of the cylinder vibrations, resulting from the translation of the construction, are such that they would not (or at least hardly) influence the shedding process.

2.2. The visualisation technique

2.2.1. The method

For the visualisations an electrolytic precipitation method is used. In this method tin-ions are separated from an anode with a layer of tin on it, by applying a voltage difference. Because the tin-ions do not dissolve in pH-neutral water, very small tinhydroxide particles (O(1 μm)) are formed, see [9]. These particles can be used to visualise the flow. In the current set-up, a flat plate (with a layer of tin on it) is positioned upstream of the cylinder and is used as an anode. The cathode, from which H_2-bubbles are separated, is placed at a position where it does not disturb the flow. The particles, separated from the flat plate form a homogeneous sheet, that moves towards the cylinder. Fig. 3a shows how the flat plate is positioned upstream of the cylinder over part of the span. The experiments, performed with this method,

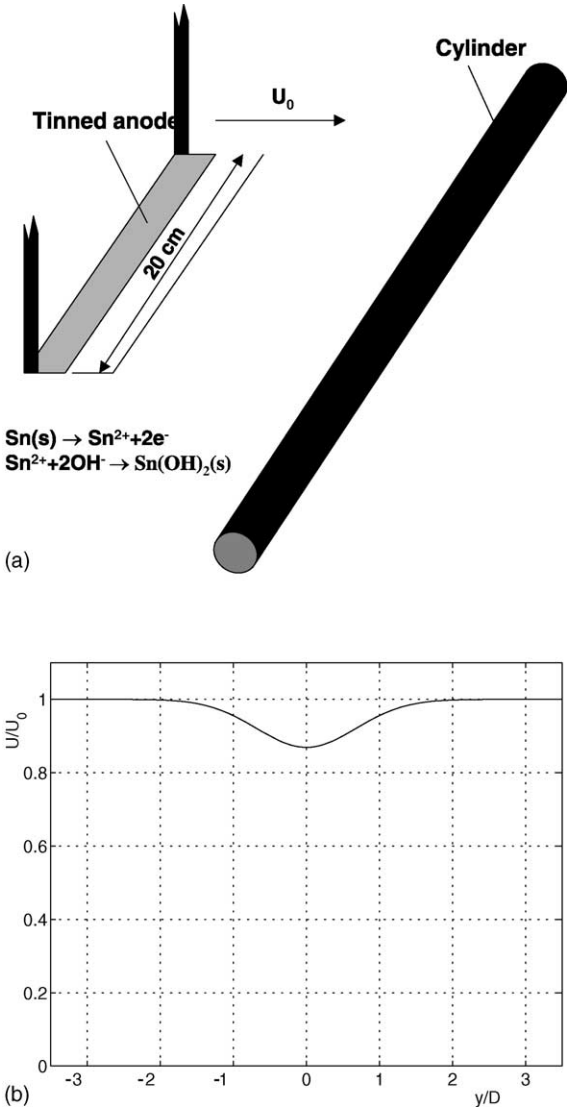

Fig. 3. Configuration of the visualisation experiment (a) and the measured velocity profile at 20 cm behind the flat plate (b).

were very reproducible when care was taken to minimise the background flow.

To visualise part of the flow, use was made of a laser sheet which cuts the wake vertically at different spanwise positions or horizontally near the centre of the cylinder. The laser sheet thickness was typically 1 mm. In this way also quantitative information could be obtained from the visualisation results.

2.2.2. Disturbance behind the flat plate

Because of the presence of the flat plate upstream of the cylinder, the flow profile at the cylinder will be disturbed. Because the background flow is deforming the visualisation sheet that moves towards the cylinder, the distance between the plate and the cylinder is limited. For an acceptable visualisation sheet at the cylinder, the maximum distance between the plate and the cylinder is found to be 20 cm for $Re_D = 117$. From PIV-measurements and a simplified theoretical model the velocity-profile at 20 cm behind the flat plate can be estimated as shown in Fig. 3b. The maximum disturbance in velocity turns out to be about 13% of the free-stream velocity at the symmetry axis and about 8% at $y/D = \pm 0.5D$. Numerical simulations show that the presence of this plate effectively leads to a decrease of Re_D of about 10% for $Ri_D = 0$. Furthermore, a variation of the distance between the plate and the cylinder in the experiments with a heated cylinder did not show any changes in the appearing structures in the vicinity of the cylinder. From these considerations it is concluded that the observed structures (which will be discussed further on) are not initiated as a result of the presence of the plate. It is worthwhile mentioning that recently employed experiments using particle tracking velocimetry (in which the plate was not present) show exactly the same structures. This is also true for recently performed 3D numerical calculations. These results, however, have not been published yet.

The Reynolds and Richardson numbers used in the rest of this paper, however, are based on the free-stream velocity (thus not corrected for the presence of the flat plate).

3. Results

Mostly, the tinned anode plate was positioned in such a way that the visualisation sheet moved through the upper boundary layer of the cylinder. To get a first impression of the occurring structures, the whole volume behind the heated cylinder was illuminated. The camera was positioned above the cylinder (with some angle with respect to the gravity vector).

The experiments show that the shed vortex rolls are 2D for $Ri_D < 0.3$ (see Fig. 4a and b for $Ri_D = 0$ and $Ri_D = 0.15$). For $Ri_D > 0.3$ 3D structures are visible in the vortex rolls as well as in the braids. These structures initially do not result in large deformations as can be seen from Fig. 4c and d for $Ri_D = 0.4$ and 0.6 respectively. In Fig. 4e for $Ri_D = 1$, some distance downstream of the cylinder the formation of thermal plumes can be seen.

The visualisations for different Ri_D at $Re_D = 102$ and 75 showed the same behaviour as for $Re_D = 117$ although the Richardson numbers at which the phenomena start and the quantitative measures may be different.

From the visualisations it appears that the flow is 3D far before the thermal plumes escape from the vortices. The three-dimensionality even seems to go back completely to the cylinder, which can be seen in Fig. 4e and, to a less extent, in d. From these figures it can be concluded that the spanwise positions, at which further downstream the thermal plumes are formed, are already determined at the rear end of the cylinder.

3.1. Vertical laser sheet intersections of the wake

In Fig. 5, experiments are shown in which the vortex street is viewed from the side and a laser sheet cuts the wake vertically at different spanwise positions for different Richardson numbers. For $Ri_D = 0$ Fig. 5a shows the von Kármán vortex street as known from literature. Fig. 5b shows the vortex street for $Ri_D = 0.2$ within the region of $x/D < 50$ behind the cylinder. In this region the vortex street shows the same behaviour at different spanwise positions, which agrees with Fig. 4b for $Ri_D = 0.15$ in which the wake also shows a 2D behaviour. For $Ri_D = 0.4$ (Fig. 5c1 and c2) the wake does show a spanwise variation. The considered region is around $50D$ again. In Fig. 5c2 the escape of a thermal plume from the upper vortex structure can be seen at about $40D$ behind the cylinder. This phenomenon is not visible in Fig. 5c1. For $Ri_D \approx 0.65$ the same process takes place as for $Ri_D = 0.4$, although the plume is formed closer behind the cylinder at ($x/D \approx 15$).

For $Ri_D = 1$ the situation changes. Instead of the thermal plumes escaping from a shed, nicely round, coherent vortex structure, a plume escapes from the braid of the upper vortex structure, straight after the vortex formation. At virtually the same moment the first plume is formed, a second plume is formed which escapes from the vortex structure itself. Fig. 5d1 and d2 show the vortex street for $Ri_D = 1$. In Fig. 5d3, in which a larger area is considered, the two thermal plumes can be seen for $Ri_D = 1.1$ at the downstream end. Fig. 5d1 clearly shows the 3D character of the flow. The picture is taken at a spanwise position between two plumes. As a result of the scattering of the light, the plumes at another spanwise position can be seen. Besides, it can be seen that the mushroom structure above the fourth upper vortex behind the cylinder, cuts through the light sheet.

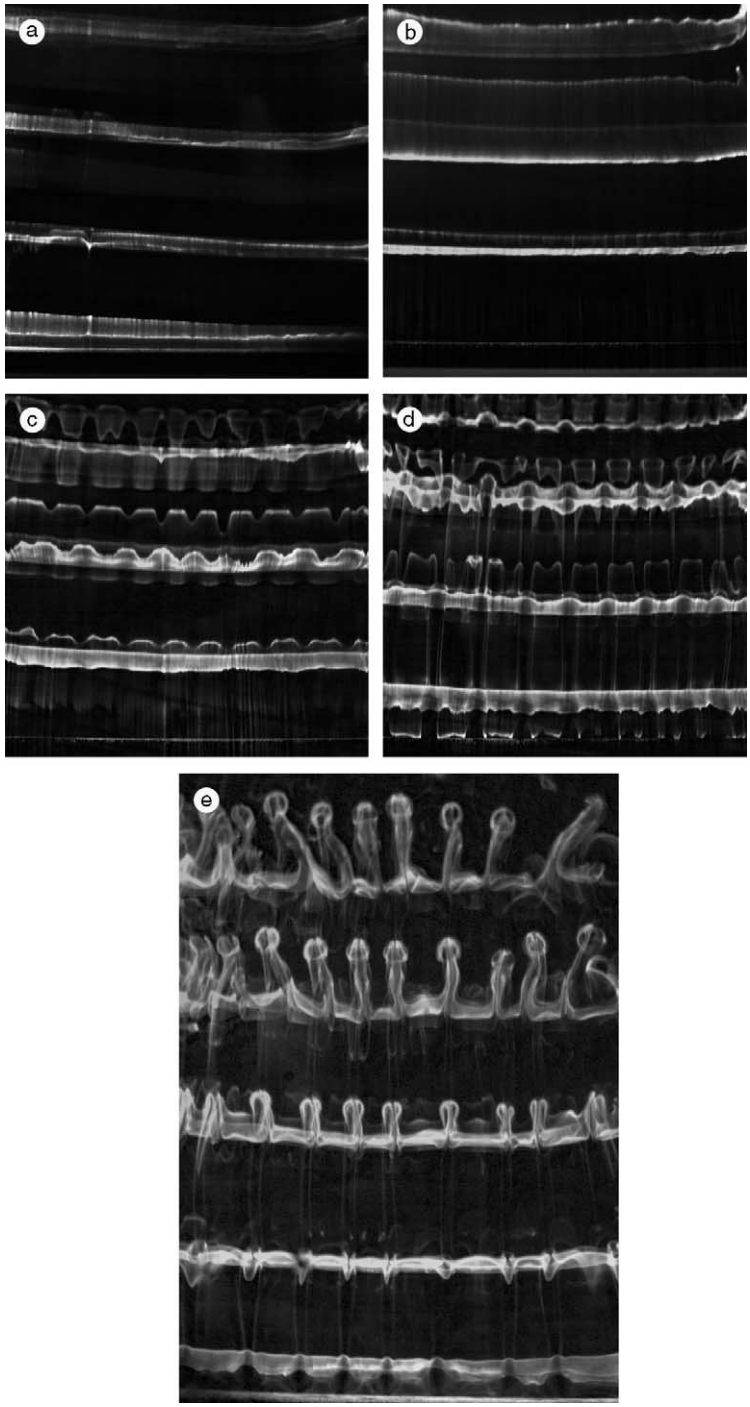

Fig. 4. Overview pictures of the vortex shedding for $Re_D = 117$ and (a) $Ri_D = 0$, (b) $Ri_D = 0.15$, (c) $Ri_D = 0.4$, (d) $Ri_D = 0.6$ and (e) $Ri_D = 1.0$. The flow is from bottom to top, the cylinder is positioned at the bottom.

Fig. 5e1 and e2 shows the vortex street for $Ri_D \approx 1.5$. Here the thermal plumes seem to escape from the vortices very close behind the cylinder, already during the vortex formation. After the escape of the plume only a very small part of the upper vortex remains. It looks like another plume is formed in the small part of the vortex that is left, some distance downstream (last vortex in Fig. 5e2).

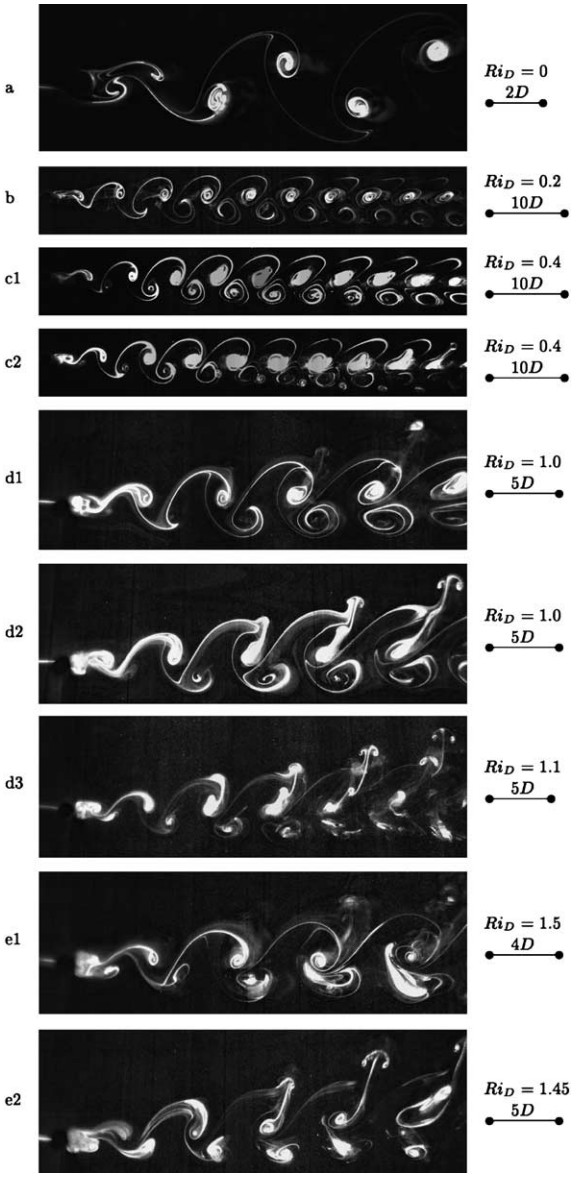

Fig. 5. Von Kármán vortex street for $Re_D = 117$ and different Ri_D. The flow is from left to right, the cylinder is positioned at the left.

In the pictures of Fig. 5, the 2D phenomena (negative deflection of the vortex street and rotation of the lower vortex underneath the upper one) described by Kieft [1] can be observed. In Fig. 5b, c1 and c2, the negative deflection of the vortex street is noticed. Furthermore, the relative motion of the upper and lower vortices, in which the lower vortex rotates in clockwise direction around the upstream upper vortex, can be seen for increasing Ri_D.

In Fig. 6 the downstream position behind the cylinder at which the plumes escape from the vortices is

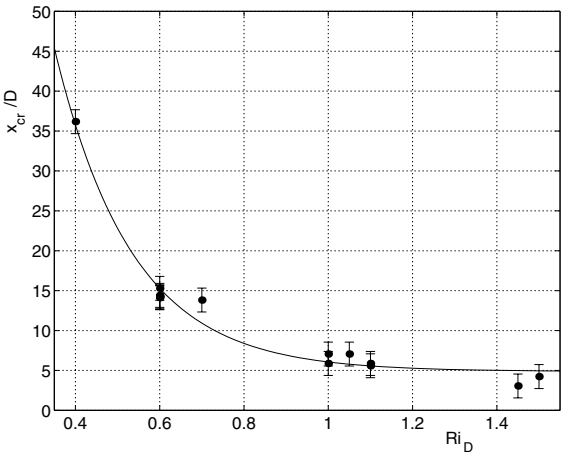

Fig. 6. Distance behind the cylinder at which the plumes escape for $Re_D = 117$ and different Ri_D.

plotted for $Re_D = 117$ as function of Ri_D. This downstream position is determined by examining a sequence of pictures, taken at a spanwise position between the plumes. Because of the scattering of the light the thermal plumes can still be seen and this way also the distance behind the cylinder at which these plumes originate, can be determined. The error that arises during the determination of the positions is estimated to be $\pm 1.5D$. Fig. 6 shows that for $Ri_D < 1$ the distance behind the cylinder at which the plumes escape, decreases fast with increasing Ri_D. For $Ri_D > 1$ the plumes are formed very close behind the cylinder and the distance seems to reach an asymptotic value of $x/D \approx 5$. For $Re_D = 75$ the same trend is seen as for $Re_D = 117$, see [3]. The difference is that for $Re_D = 75$ the asymptotic value is at $x/D \approx 13$ and is reached approximately for $Ri_D \approx 1.5$ instead of 1.

3.2. Horizontal laser sheet intersections of the wake

To study the wake behind the cylinder in more detail, the wake is cut by a horizontal laser sheet, just above the centre of the cylinder. The camera is positioned above the wake (viewing from the top) and the visualisation sheet moves through the upper boundary layer again. In Fig. 7 it can be seen that for $Ri_D = 0$ and 0.15, the wake is 2D (except for the fact that for $Ri_D = 0.15$, just as for $Ri_D = 0.35$ and 0.6, some oblique shedding [7] occurs). For $Ri_D = 0.35$, 0.6 and 1, 3D structures are observed at the rear end of the cylinder. These structures appear for $Ri_D > 0.3$. This is the same Richardson number as for which the formation of thermal plumes at certain spanwise positions is visible in the vertical laser sheet intersections, and for which the overview pictures show a 3D behaviour.

Although less clear than in the horizontal intersections, the 3D structures are also visible in Fig. 4e,

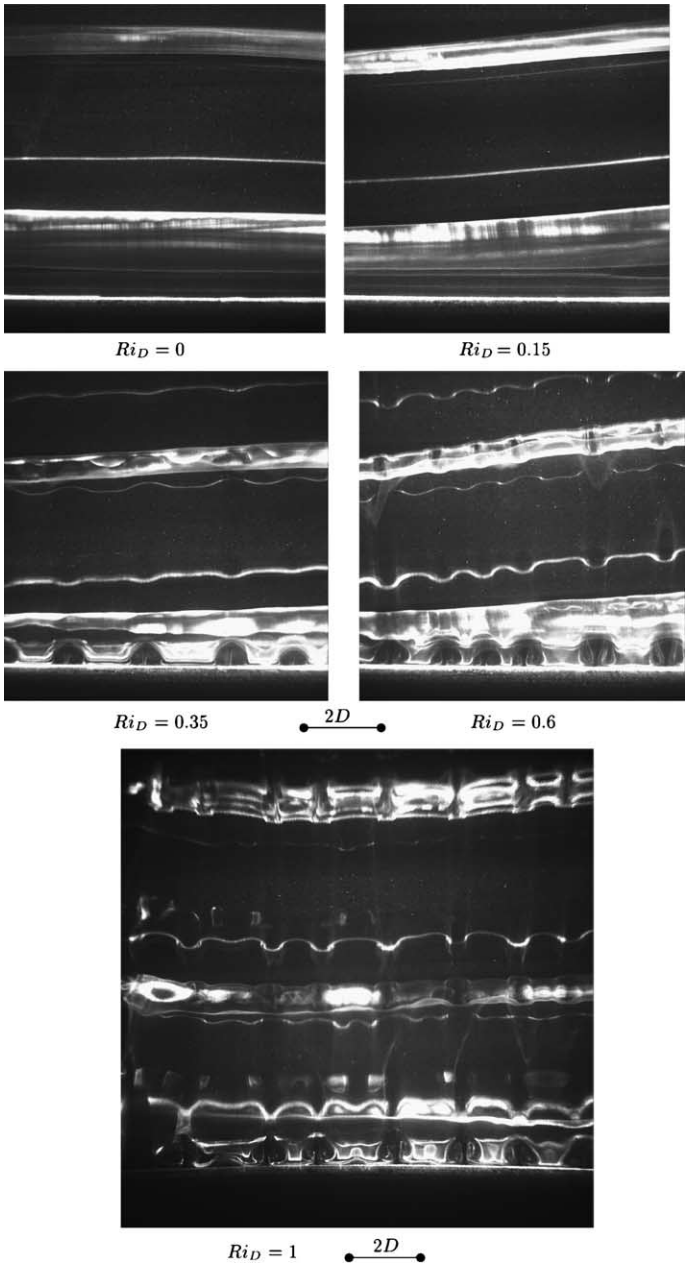

Fig. 7. Horizontal intersection of the wake at $Re_D = 117$ and different Ri_D. The flow is from bottom to top, the cylinder is positioned at the bottom.

where the whole volume behind the cylinder was illuminated. The spanwise positions at which these structures appear are exactly those at which further downstream the thermal plumes escape. Instead of a two-dimensionally shed vortex roll from which further downstream the plumes escape, the three-dimensionality appears to be present already at the rear end of the cylinder.

In Fig. 8 a snapshot is given of the 3D structure at the rear end of the cylinder for $Re_D = 117$ and $Ri_D = 1$. The 'vortical structure' manifests itself as two counter-rotating vortices. From the visualisations it followed that at the moment the upper vortices are shed, fluid is convected towards the spanwise positions at which further downstream the plumes are formed (indicated in Fig. 8 with the arrows).

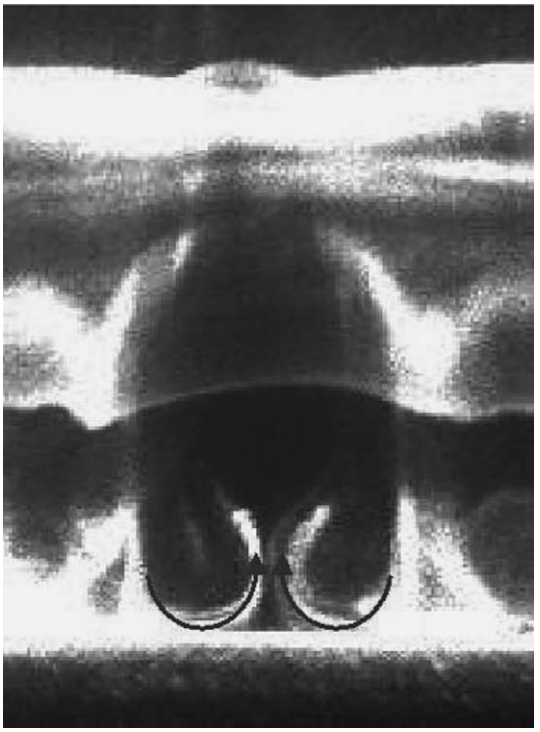

Fig. 8. Vortical structure at the rear end of the cylinder for $Re_D = 117$ and $Ri_D = 1$. The flow is from bottom to top, the cylinder is positioned at the bottom.

3.3. Quantitative data

From the overview pictures and the horizontal wake intersections, the spanwise wavelength of the 'instability' can be determined. This is done by averaging the wavelength over 20 cm of the span plus averaging over a few moments in time within an experiment. Fig. 9a shows the result of this. Beside $Re_D = 117$ also some experiments with $Re_D = 102$ and 75 are included. [1] It appears that the wavelength for different values of Ri_D is fairly close to the average wavelength (wavelength averaged over different experiments at $Re_D = 117$). This is also true for the wavelengths determined at $Re_D = 102$ and 75. So, in the investigated area, the wavelength of the 'instability' seems to be fairly independent of Re_D and Ri_D and equals $1.8D$.

In Fig. 9b, the Strouhal frequency, $St = fD/U_0$, is plotted against Ri_D, for $Re_D = 117$. Through the data a quadratic function is fitted (expression not given here). The shedding frequency was determined at $15D$ behind the cylinder. Due to the finite frame-rate, the inaccuracy of the velocity determination and the possible occurrence of oblique shedding, the accuracy of St is estimated to be (+6.0%, −2.5%). The maximum difference between the measured Strouhal frequencies is about 20%, from which it can be concluded that St increases with increasing Ri_D. From the 2D numerical calculations of Kieft [2] a slight decrease of St followed. It should be noted that in those calculations no temperature dependency of the viscosity was considered. In Appendix A a possible explanation will be given for these observations. Here also the concept of using an effective Reynolds number Re_{eff}, as employed in [12,13], will be considered.

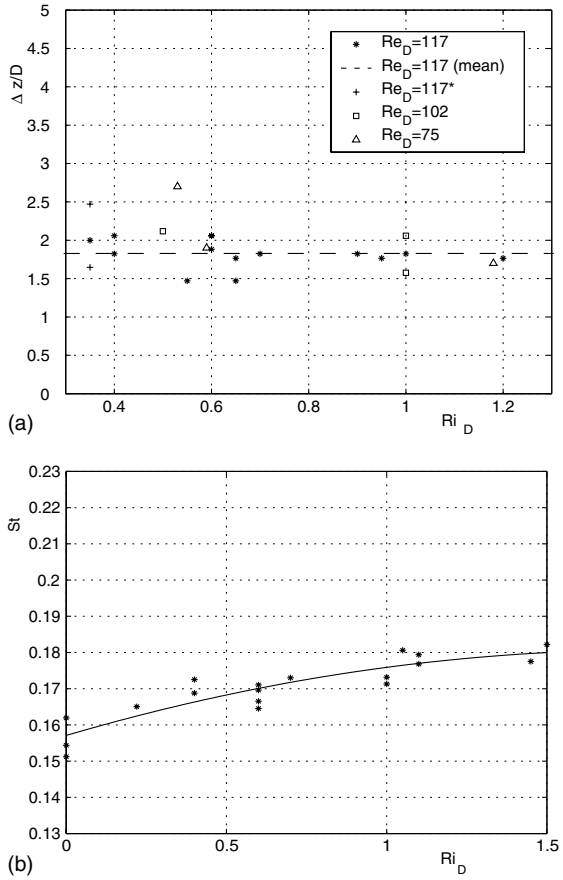

Fig. 9. Spanwise distance Δz between the 3D-structures for $Re_D = 117$, 102 and 75 and different Ri_D (a) and Strouhal frequency St for $Re_D = 117$ and different Ri_D (b).

4. Discussion

4.1. Influence of the upward buoyancy force on the vortex formation

The similarity between the advection of wall-vorticity and warm fluid results in hot isolated 'blobs' that coin-

[1] At two of the measurements at $Re_D = 117$ and $Ri_D = 0.35(+)$, the 'instability' was only present over a small part of the span. Here the wavelength is averaged over this part only.

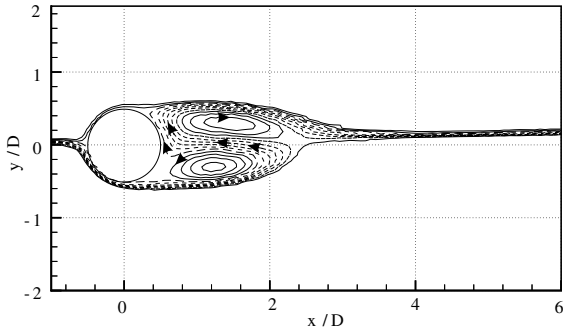

Fig. 10. Calculated averaged streamline pattern for $Re_D = 75$ and $Ri_D = 0.5$ [2].

cide with the vortex structures [3]. Because the warm fluid is captured in the kernel of the vortex structures, only diffusion processes can cause the hot blob to spread. As diffusion takes place relatively slow, the hot blob is preserved until the vortex becomes unstable. Furthermore the convection of heat to the vortices behind the heated cylinder is such that the upper vortices become warmer than the lower ones [6]. One of the reasons for this is that the upper vortices are formed closer to the cylinder (the main reason for this is that negative baroclinic vorticity production delays the formation of the positive lower vortices). Secondly, it appears that part of the heat that is convected to the upper vortices comes from the lower wake-half. Both of these mechanisms are also clearly seen in Fig. 10, where the average streamline pattern is shown for $Re_D = 75$ and $Ri_D = 0.5$ (results obtained with a 2D numerical simulation based on a spectral element method [2]). The downward shift of the stagnation point at the back of the cylinder is a result of the upward buoyancy force of the warm fluid behind the cylinder.

For the current problem it can be stated that the transport of warm fluid is dominated by convection, as $Re_D Pr \gg 1$. Heat is added to the flow at the cylinder walls. In the experiments, it was attempted to position the visualisation sheet in the boundary layer, as close to the cylinder as possible. This means that for a qualitative consideration, it can be assumed that the transport of the visualisation particles and warm fluid are analogous. As mentioned, Kieft [3] concluded that most of the hot fluid was being captured in the coherent vortex structures. This can also be seen in Fig. 5 for $Ri_D < 1$. Here, nicely round vortices are shed from which further downstream the thermal plumes escape. For $Ri_D > 1$ the situation changes. Instead of a nicely round vortex, the visualisation dye (and so the warm fluid) is shifted upward (see Fig. 5 for $Ri_D > 1$). Instead of the plumes escaping from a coherent shed structure, the thermal plume escapes shortly after or already during the vortex formation. This can best be seen from the camera recordings, but it can also be noticed in Fig. 5e2 for $Ri_D = 1.45$. It seems that for $Ri_D > 1$ the upward buoyancy force of the warm fluid prevents the formation of coherent vortex structures.

In Fig. 6 it can be observed that for $Ri_D > 1$ and $Re_D = 117$ the plumes are formed very close to the cylinder and an asymptotic value is reached. As mentioned before, for $Re_D = 75$ the same trend is seen except that the asymptotic value is larger. The higher asymptotic value can probably be explained by the increasing vortex formation length with decreasing Re_D, so the hot fluid is collected further downstream. Besides, the determination of x_{cr}/D in the present investigation is based on visualisation results, whereas the method used by Kieft [3] was based on velocity measurements.

4.2. The 'instability' behind the cylinder

As mentioned before, the spanwise positions at which the thermal plumes are formed, seem to be determined at the rear end of the cylinder. In the previous section it was described that the occurring 'vortical structures' result in a transport of fluid at the back of the cylinder, towards the spanwise positions at which further downstream the plumes are formed. Because the fluid temperature is at its highest at the back of the cylinder, this means a transport of warm fluid to these spanwise positions.

In Fig. 11a, visualisations are shown in which the visualisation sheet is positioned in the upper boundary layer over one part of the span and in the lower boundary layer over the other part of the span. Here it can be seen that in the part in which the visualisation sheet is at the upper side of the cylinder, most of the dye ends up in the upper vortices. Over the other part of the span, most of the dye flows to the lower vortices, except at the spanwise positions at which further downstream plumes are formed. At these positions also a considerable part of the dye ends up in the upper vortices (this is why further downstream, also over this part of the span, the plumes can be seen).

From the 2D numerical calculations of Kieft [2], it followed that there was a net transport of fluid from the lower to the upper wake half (see also Fig. 10). From the current visualisations it follows that this net transport is enhanced at certain spanwise positions. This may lead to a spanwise variation in the temperature of the upper vortex roll. This is confirmed in Fig. 11b and c in which vertical intersections of the wake at different spanwise positions are shown for $Re_D = 117$ and $Ri_D = 1$. Here it is seen that at a spanwise position at which plumes are formed (Fig. 11c) considerably more visualisation dye, and so warm fluid, is present in the upper vortices than at a spanwise position between the thermal plumes (Fig. 11b).

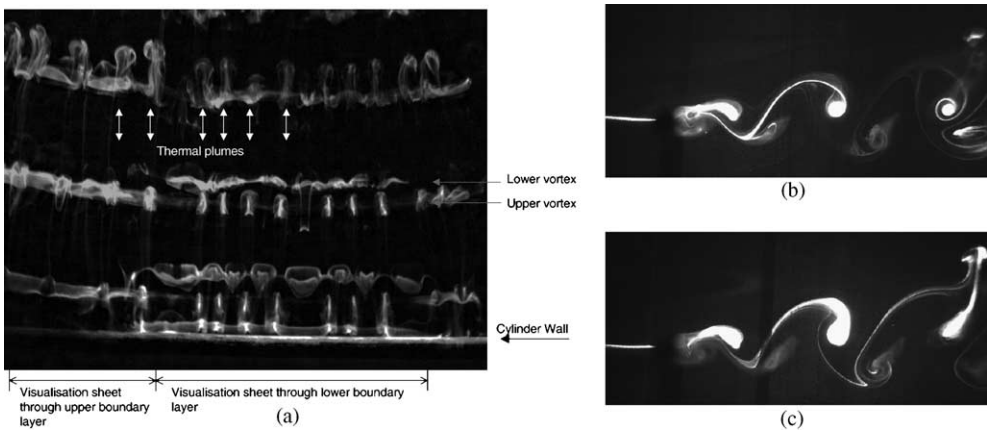

Fig. 11. Visualisation in which the visualisation sheet moves partly under and partly over the cylinder (a: flow from bottom to top) and the convection of visualisation particles *between* (b: flow from left to right) and *in* (c: flow from left to right) the thermal plumes for $Re_D = 117$ and $Ri_D = 1$.

In Fig. 12a a schematic presentation of the net transport of hot fluid is given. As a result of the spanwise temperature gradients, there will be baroclinic vorticity production, which equals $Ri_D \nabla \Theta \times \mathbf{g}$ (see Eq. (4)), perpendicular to the vortex rolls. This is shown in Fig. 12b. Although small, this vorticity perpendicular to the vortex rolls can also be seen in Fig. 13a, in which a horizontal laser sheet intersection cuts, respectively (in downstream direction), through an upper vortex roll, the upper braid, the lower braid and an upper vortex again. With Fig. 13b it can be deduced that the sign of this vorticity corresponds with the situation as sketched in Fig. 12b. Possibly the curvature of the braids is the result of the above mentioned baroclinic vorticity production. It is also possible that this curvature is created by the 3D velocity field, present at the rear end of the cylinder (convection of vorticity). This needs to be clarified by numerical calculations.

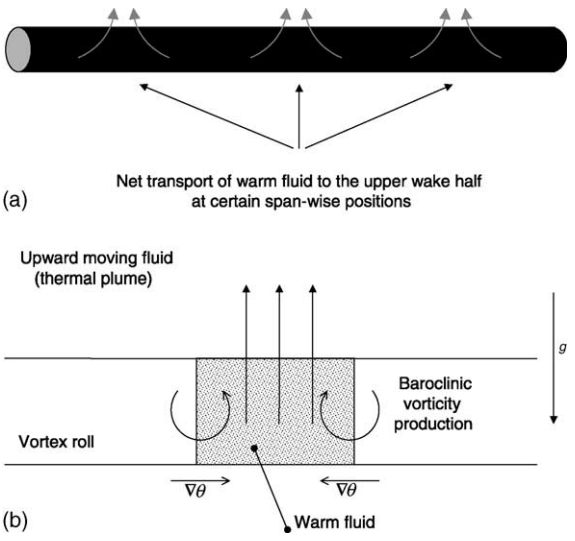

Fig. 12. Possible form of the 'instability' at the back of the cylinder (a) and the resulting spanwise variation of the vortex temperature (b).

For $Ri_D > 1$, besides the mentioned curvature in the braids, also larger 3D structures ('blobs-in-pairs') situated under the braids (see Fig. 14) and a spanwise variation in the braid thickness (compare Fig. 5e1 and e2) are visible. The 'blobs-in-pairs' and the variation in the braid thickness appear with the same wavelength as the aforementioned 'instability' and, so, are probably related to it. The 'blobs-in-pairs', however, were not always as clearly visible as presented in Fig. 14. Therefore, they need to be studied in more detail (for example by visualising with horizontal intersections at higher Ri_D).

With the schematic presentation of the net transport of fluid, given in Fig. 12a, a possible explanation can be given for the flow visualisation results as presented in the overview pictures of Fig. 4, up to the position where the plumes escape from the upper vortex roll. Fig. 15a gives an overview picture again of the flow visualisation at $Re_D = 117$ and $Ri_D = 0.6$. In Fig. 15b a side view is presented of the same situation. The scattering of light makes it possible to see the situation at different spanwise positions. It may be concluded that the rotation velocity of the lower vortices at the spanwise positions at which the plumes are formed is less than over the rest of the span. Possibly the above mentioned net transport of fluid from lower to upper wake half at these spanwise positions disturbs the convection of vorticity to the lower vortices, resulting in a strength variation along the lower vortex roll. This, on its turn, may lead to the 'wavy structures' as observed in the visualisation results.

Visualisations of the flow in the vicinity of the cylinder at $Re_D = 75$ and 102, showed that also for these

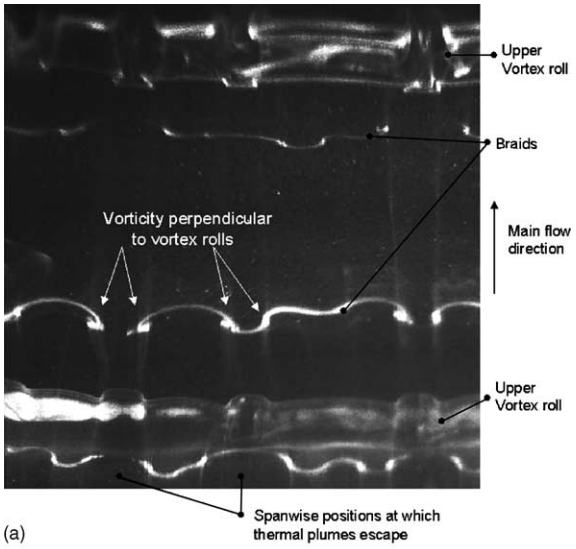

Fig. 13. Vorticity in the braids, perpendicular to the vortex rolls, in a horizontal intersection (a: flow from bottom to top) and in an overview illustration (b: flow from left to right).

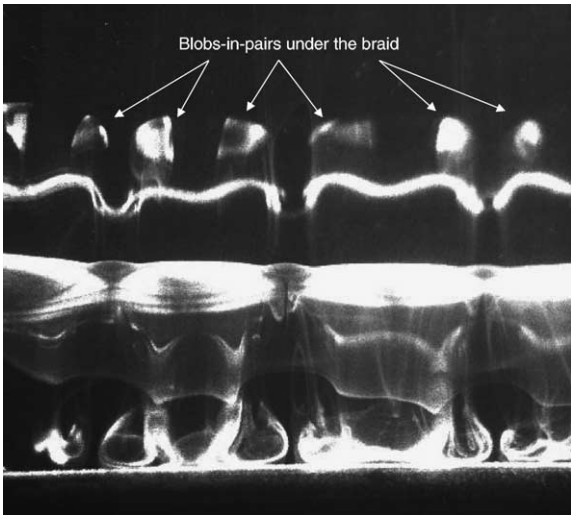

Fig. 14. Visualisation showing the blobs-in-pairs for $Re_D = 117$ and $Ri_D = 1$ (flow from bottom to top).

Reynolds values 'vortical structures' behind the cylinder are present for $Ri_D < 1$ (experiments were taken at $Ri_D = 0.5$). In view of the fact that these structures seem to be directly related to the formation of thermal plumes further downstream for $Re_D = 117$, this plume formation probably also occurs for $Ri_D < 1$ at $Re_D = 75$ and $Re_D = 102$. However, in his velocity measurements at $Re_D = 75$, Kieft [3] measured up to $x/D = 25$ and concluded from the results that the vortex street remained 2D for $Ri_D < 1$. From his results it can be deduced that if thermal plumes are formed for $Ri_D < 1$, this will be for $x/D > 25$. Because the visualisations show an integrated effect of the occurring 3D structures during their downstream convection, it can be concluded that for these smaller Reynolds values these structures do not result in large deformations. Apparently, the spanwise variations that result from the three-dimensionalities

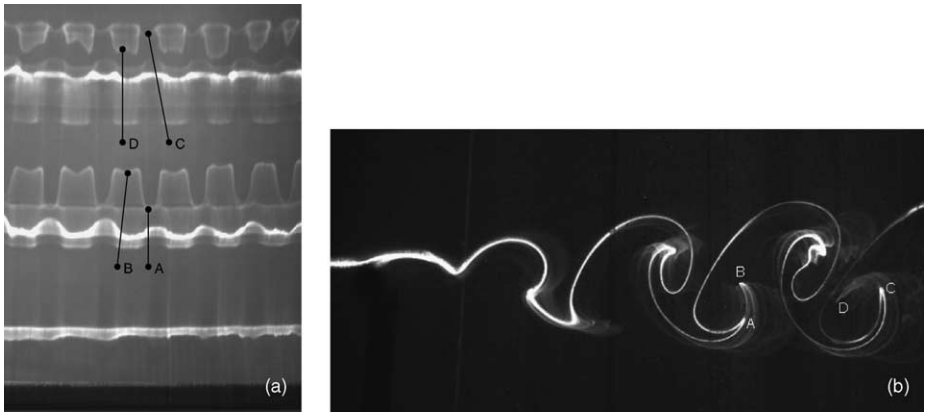

Fig. 15. Spanwise variation of the circulation velocity in an overview picture (a: flow from bottom to top) and in a side view picture (b: flow from left to right) for $Re_D = 117$ and $Ri_D = 0.6$.

were in that case of the same order of magnitude as the (assumed) inaccuracy of the velocity measurements or as the background flow, making a 2D flow description quite justifiable.

5. Conclusions

In the present study the wake flow behind a heated cylinder is investigated at $Re_D = 117$ and various Richardson numbers. The wake becomes 3D for $Ri_D > 0.3$. For these Richardson numbers 3D 'vortical structures' are observed near the cylinder wall. Here already the spanwise positions, at which further downstream the plumes are formed, are determined. For $Ri_D < 1$ the warm fluid is collected in the coherent vortex structures from which further downstream the thermal plumes escape. For $Ri_D > 1$, the upward buoyancy force seems to prevent the formation of coherent vortex structures and the plumes already escape at the vortex formation position, very close to the cylinder.

It seems that the 'vortical structures' behind the cylinder result in an extra transport of warm fluid to the upper vortices at certain spanwise positions. This results in spanwise temperature variations in the upper vortex roll, possibly leading to baroclinic vorticity production. The net transport of hot fluid from lower to upper wake half also seems to disturb the advection of vorticity to the lower vortices, which, on its turn, results in a spanwise variation of the vortex strength.

Although 3D structures in the wake are present far before the formation of the plumes, the velocities associated with these structures are small. For this reason, a 2D consideration of the wake describes the occurring phenomena, like a negative deflection of the vortex street and the relative motion of the vortices, very well.

In future research, temperature measurements in a cross-section of the upper vortex roll are aimed at, to confirm (or reject) the spanwise temperature gradient hypothesis. The laser induced fluorescence technique, as performed in [6], can be used for that. Furthermore the exact source of the 'instability' should be investigated like Williamson [5] did for the purely forced convection case. Besides, it may be interesting to perform 3D velocity measurements to examine the occurring 'vortical structures' and to study the spanwise variations in vortex strengths. Also the observed 'blobs-in-pairs' occurring for higher Ri_D, need some further examination.

Appendix A. The influence of cylinder heating on the Strouhal frequency

As mentioned in the results section the Strouhal frequency in the experiments seems to increase with increasing Richardson number, which is in contrast with the 2D numerical calculations performed by Kieft [2]. The maximum increase of St in the experimental data is 20% of which a maximum of 8.5% could be the result of experimental inaccuracies.

In [12,13] the effect of cylinder heating on the laminar vortex shedding of an air flow behind a circular cylinder has been investigated. It followed that by defining an effective Reynolds number based on an effective temperature of $T_{\text{eff}} = T_\infty + 0.28(T_w - T_\infty)$, the St–Re curve as found for the flow behind an unheated cylinder is also applicable for the flow behind a heated cylinder, even for very high temperature differences. When this effective temperature concept is applied to the current problem, a rise of St from $Ri_D = 0$ to $Ri_D = 1.5$ of approximately 5% is estimated. Together with the experimental inaccuracies this is appreciably less than the estimated 20%. It should be noted that all the studies on the effective Reynolds number were in the forced convection regime ($Ri < 0.05$), this in contrast to the present study.

From the above mentioned it follows that the increase in the Strouhal number as function of the Richardson number can not be fully attributed to experimental inaccuracies and/or temperature dependent material properties. Another possible explanation may be sought in the early transition towards 3D. A model is used that was presented by Roshko [10], with which the changes in the flow structures in the wake can be considered.

When the average streamline pattern is considered, the recirculating region (the wake) is enclosed by the so called zero streamline $\psi = 0$ (see Fig. 16a). Assuming constant base pressure throughout the wake and along the free streamlines and making assumptions about the shape of the wake, the wake length can be related to the base pressure. Qualitatively it follows that a decreasing base pressure results in a decreasing wake length (a lower base pressure will force the fluid outside of the wake, towards the symmetry axis faster). In Fig. 16b this is quantitatively shown by line b) (from [10]).

The base pressure is determined by the distribution of shear stress and pressure in the wake. In this analysis the conservation of momentum is approximated by (see also the illustration in Fig. 16b),

$$\oint_{\psi=0} p\,\mathrm{d}y + \oint_{\psi=0} \tau\,\mathrm{d}x \approx (p_b - p_0)d + 2\tau L = 0. \tag{5}$$

In the stationary regime τ equals the viscous shear stress along the zero streamline. For higher Re_D, the Reynolds stress (which is the result of the instationary transport of momentum over the boundaries) will increasingly take over. Depending on τ, from Eq. (5) also a relation between the wake length and the base pressure can be deduced (line c for lower, and line d for higher Reynolds stresses). By combining the above described relations between base pressure and wake length, both of these quantities can be determined. Furthermore it should be mentioned that in [11], Roshko found that the shedding

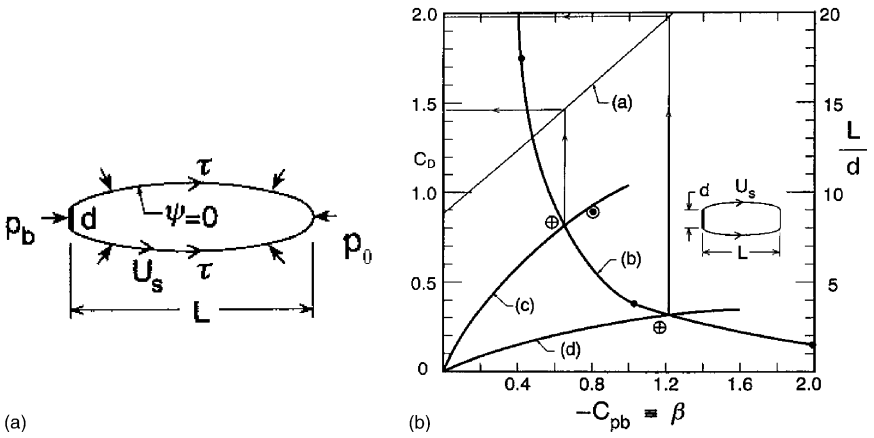

Fig. 16. Definition of the average wake (a) and the determination of the wake length (b) [10].

frequency was approximately inversely proportional to the wake length.

The above derived equations are based on the fact that the average wake was closed. As shown in Fig. 10 in the introduction, it follows from the 2D numerical calculations that the average wake is not closed, when the cylinder is heated. In case we do define a closed contour for this situation, like for example the zero streamline as defined for $Ri_D = 0$, there will be a net transport of momentum over this boundary. For Eq. (5) this results in a positive term for the transport of momentum on the right-hand side: $\oint_{\psi=0} \rho u_x(\mathbf{u}\cdot\mathbf{n})\,ds$. For the equation to hold, the wake length, L, should increase and/or the base pressure, p_b, should increase (corresponding to a decrease of $-p_b$). As mentioned above and as shown by line b in Fig. 16, an increasing base pressure directly relates to an increasing wake length. From this it follows that purely as a result of the average transport of momentum from the wake, the wake length will increase. As mentioned, this increase of wake length will lead to a decrease of the shedding frequency. It is very well possible that the net transport of momentum from the wake, which on its turn is a result of the net transport from lower to upper wake half, causes the decreasing shedding frequency in the 2D numerical calculations, in which both the temperature dependent viscosity and 3D effects were not taken into account. From the experiments an increase of shedding frequency followed. The difference with the numerical calculations is the temperature dependent viscosity (of which its effect on the Strouhal frequency is already discussed) and the occurrence of 3D structures. Probably (see also Fig. 16b, lines c and d) the 3D structures result in an increase of the Reynolds stresses (averaged over the span), which cause a decrease in wake length and an increase in shedding frequency.

References

[1] R.N. Kieft, C.C.M. Rindt, A.A. van Steenhoven, The wake behaviour behind a heated horizontal cylinder, Exp. Therm. Fluid Sci. 19 (1999) 183–1511.
[2] R.N. Kieft, Mixed convection behind a heated cylinder, Ph.D. thesis, University of Technology Eindhoven, 2000.
[3] R.N. Kieft, C.C.M. Rindt, A.A. van Steenhoven, Heat induced transition of stable vortex street, Int. J. Heat Mass Transfer 45 (2002) 2739–2753.
[4] D. Gray, A. Giorgini, The validity of the Boussinesq approximation for liquids and gasses, Int. J. Heat Mass Transfer 19 (1976) 545–551.
[5] C.H.K. Williamson, Three-dimensional wake transition, J. Fluid Mech. 328 (1996) 345–407.
[6] H.J. Seuntiëns, R.N. Kieft, C.C.M. Rindt, A.A. van Steenhoven, 2-D temperature measurements in the wake of a heated cylinder using LIF, Exp. Fluids 31 (2001) 588–595.
[7] C.H.K. Williamson, Oblique and parallel modes of vortex shedding in the wake of a circular cylinder at low Reynolds number, J. Fluid Mech. 206 (1989) 579–627.
[8] M. Nishioka, H. Sato, Measurements of velocity distributions in the wake of a circular cylinder at low Reynolds numbers, J. Fluid Mech. 65 (1974) 97–112.
[9] S. Taneda, H. Honji, H. Tatsuno, The electrolytic precipitation method of flow visualisation, in: The International Symposium on Flow Visualisation, 1977, pp. 133–138.
[10] A. Roshko, Perspectives on bluff body aerodynamics, J. Wind Engng. Indust. Aerodyn. 49 (1993) 79–100.
[11] A. Roshko, On the wake and drag of bluff bodies, J. Aeronaut. Sci. 22 (1955) 124.
[12] F. Dumouchel, J.C. Lecordier, P. Paranthoën, The effective Reynolds number of a heated cylinder, Int. J. Heat Mass Transfer 41 (1998) 1787–1794.
[13] A.B. Wang, Z. Trávníček, K.C. Chia, On the relationship of effective Reynolds number and Strouhal number for the laminar vortex shedding of a heated circular cylinder, Phys. Fluids 12 (2000) 1401–1410.